



ELSEVIER

Available online at www.sciencedirect.com

SCIENCE @ DIRECT®

International Journal of Multiphase Flow 31 (2005) 969–995

International Journal of
**Multiphase
Flow**

www.elsevier.com/locate/ijmulflow

Shock wave refraction patterns at interfaces

R.R. Nourgaliev *, S.Y. Sushchikh, T.N. Dinh, T.G. Theofanous

Center for Risk Studies and Safety, University of California, Santa Barbara, USA

Received 25 January 2005; received in revised form 25 April 2005

Abstract

Interactions of shock waves with gas–gas and gas–liquid interfaces (under both slow–fast and fast–slow configurations) are studied using the recently developed Adaptive Characteristics-based Matching (aCBM) method for capturing interfaces in compressible multi-fluid media. First, we verify our approach for the gas–gas case; a class of problems for which a substantial body of knowledge already exists. Then, we consider slow–fast, gas–liquid interfaces under weak shocks, and fast–slow, liquid–gas interfaces under strong shocks. The very high acoustic impedance mismatch situation here creates significant numerical (simulation) and experimental (visualization) difficulties, and the literature for it is meager and sporadic. Compared to gas–gas interfaces we note both similarities and differences. We discuss the sources for these differences, as well as potential implications of generalizing and embedding such results in multi-dimensional simulation schemes towards improving their front-capturing performance.

© 2005 Elsevier Ltd. All rights reserved.

Keywords: Shock waves; Compressible multi-phase flows; Shock refraction; Characteristics-based methods; Front capturing; Level set; Adaptive mesh refinement; Interfacial instability

* Corresponding author.

E-mail addresses: robert@engr.ucsb.edu (R.R. Nourgaliev), sveta@engr.ucsb.edu (S.Y. Sushchikh), nam@engr.ucsb.edu (T.N. Dinh), theo@engr.ucsb.edu (T.G. Theofanous).

1. Introduction

When a shock wave hits a multi-material interface in compressible media it is refracted, forming a *refraction pattern*. Depending on the acoustic impedances of the media, and geometry of the interface, the angle of the attack β , and the strength of the shock (expressed by the shock Mach number M_{sh} in the incident medium), the incident and transmitted shocks, together with the reflected wave, may form either a *regular* (single refraction node) *pattern*, Fig. 1, or a variety of *irregular* (complex) *refraction patterns* (Henderson, 1966, 1989). An irregular wave pattern results from breakdown of the local description of an elementary wave pattern in terms of steady supersonic flows. Understanding the physics of such pattern formation and its effects on interface evolution has long been a subject of research, using combinations of theory (von Neumann, 1943; Whitham, 1958, 1959; Henderson, 1966; Catherasoo and Sturtevant, 1983; Schwendeman, 1988), experiments (Jahn, 1956; Abd-El-Fattah et al., 1976; Abd-El-Fattah and Henderson, 1978a,b; Haas and Sturtevant, 1987; Bourne and Field, 1992; Igra and Takayama, 2003; Takayama, 1987) and numerical simulations (Grove and Menikoff, 1990; Henderson et al., 1991; Liu et al., 2001). Such phenomena take place in numerous settings, a small sampling of which is illustrated in Figs. 2–5. Of current interest are numerical simulations in several areas, including inertial confinement fusion, underwater explosions, atmospheric dissemination of chemical agents, com-

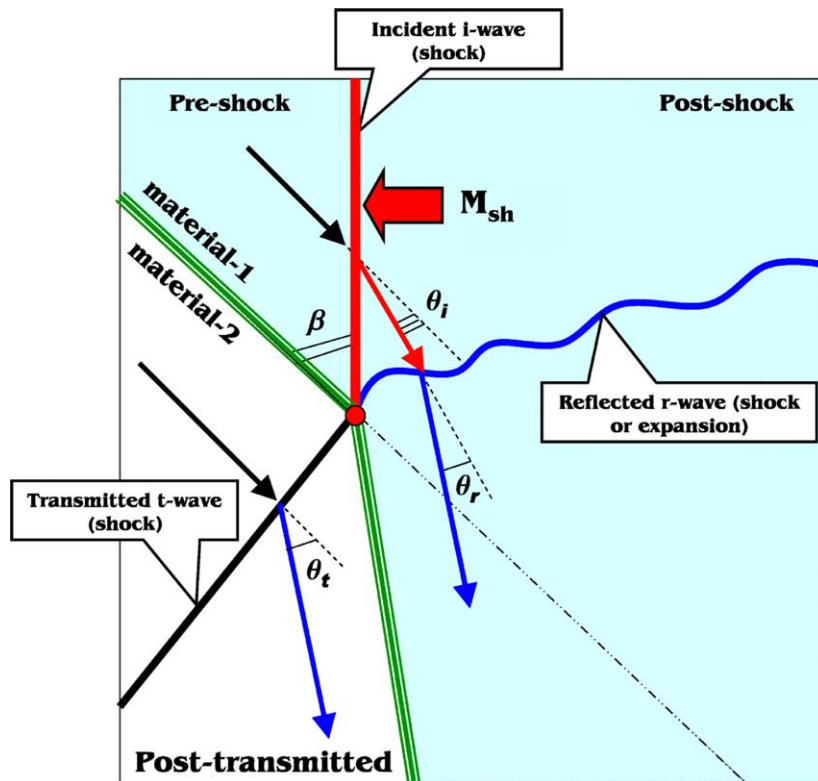


Fig. 1. Regular refraction pattern.

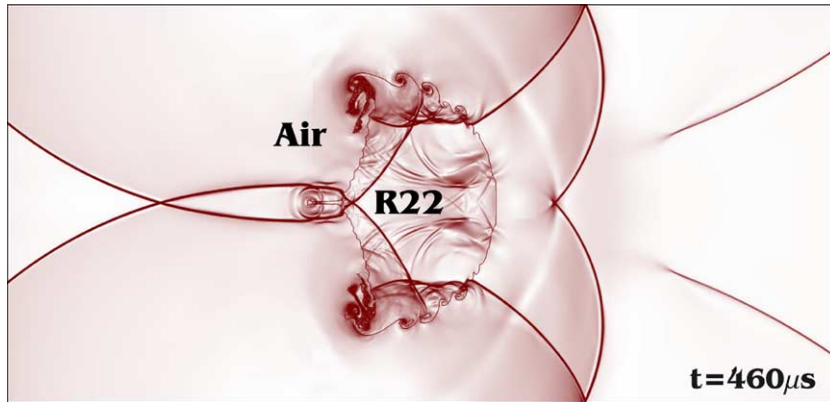


Fig. 2. Interface deformation and shock refraction for a fast–slow interface between air and bubble of refrigerant R_{22} . Numerical Schlieren from a simulation of Haas and Sturtevant’s (1987) experiment. The shock propagates from right to left. Numerical Schlieren is computed with Eq. (2), using $\kappa = 2000$ and 400 for air and R_{22} , respectively.

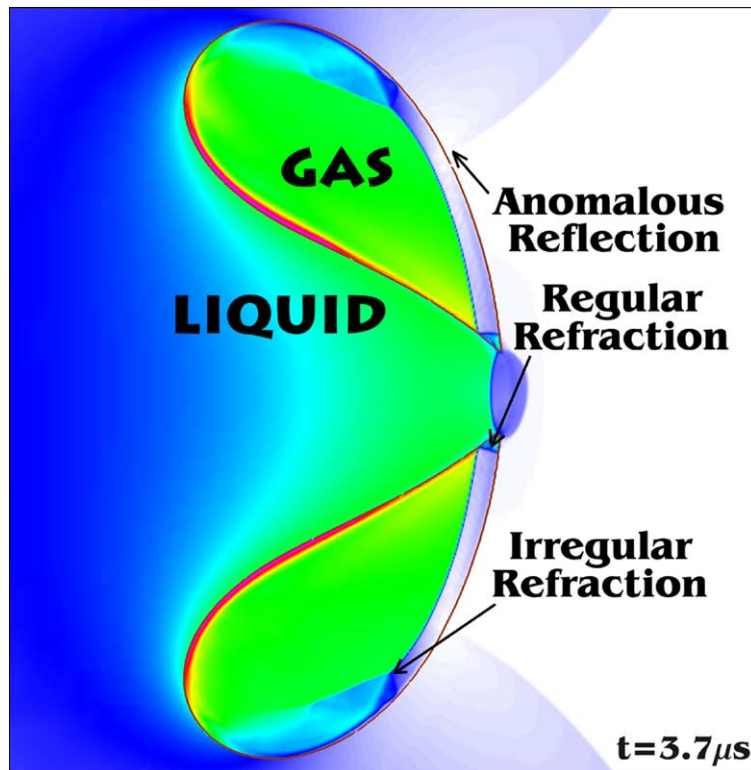


Fig. 3. Shock refraction at a gas–liquid interface for a shock-induced bubble collapse problem. Mach number field from a numerical simulation. The shock propagates from left to right.

bustion of liquid fuels, and interaction of shock waves with bubbly media (Theofanous et al., 2004).

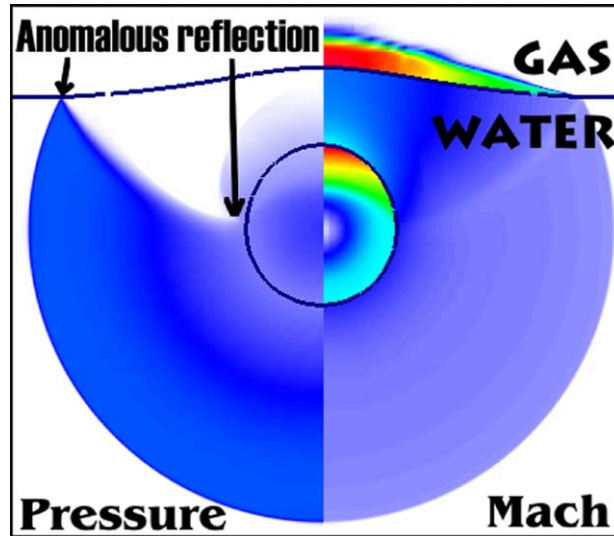


Fig. 4. Anomalous reflection at a gas–liquid interface for an underwater explosion problem. Numerical simulation (present study).

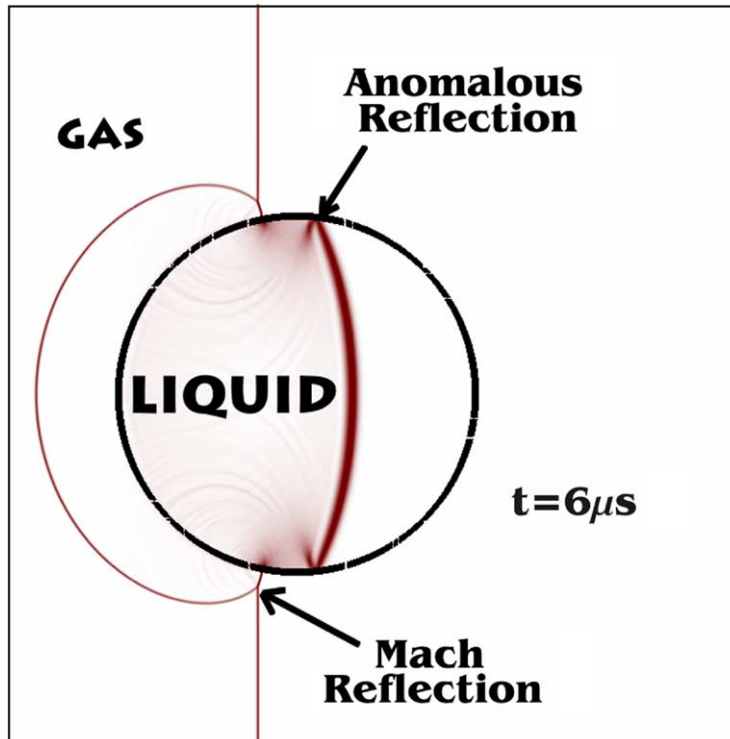


Fig. 5. Refraction patterns at a gas–liquid interface for a shock–liquid drop interaction. Numerical Schlieren is computed with Eq. (2), using $\kappa = 10^5$ and 500 for liquid and gas, respectively. The shock propagates from left to right.

The earliest experimental studies of shock refractions at gas–gas interfaces are due to Jahn (1956), while a systematic experimental investigation of irregular refraction on a gaseous interface was carried out by Abd-El-Fattah et al. (1976) and Abd-El-Fattah and Henderson (1978a,b). Based on the combinations of materials across the interface, the shock-interface interactions were separated into two major groups: “slow–fast” and “fast–slow”, the speeds referring to the acoustic impedances (ρc) of the materials involved, while the order is to denote the direction of propagation of the shock. Within each group, the interactions were further subdivided into sub-classes, in terms of (i) *Very Weak*, (ii) *Weak*, (iii) *Strong* and (iv) *Stronger* incident shocks for fast–slow interfaces (Abd-El-Fattah and Henderson, 1978a); and (i) *Very Weak*, (ii) *Weak* and (iii) *Strong* incident shocks for slow–fast interfaces (Abd-El-Fattah and Henderson, 1978b). Running experiments under different conditions, Abd-El-Fattah and Henderson have observed eight and four distinct patterns for slow–fast (Abd-El-Fattah and Henderson, 1978b) and fast–slow (Abd-El-Fattah and Henderson, 1978a) interfaces, respectively, as summarized in Table 1. The results were depicted in regime maps, which define the domains of a particular pattern’s existence on the (strength of the shock) – (incident shock angle of attack) plane.

Experiments with gas–liquid interfaces are very difficult, and those few that exist are of rather limited scope. For the slow–fast case we have Takayama and co-authors who employed double-exposure holographic interferometry to visualize shock interaction with planar (Takayama, 1987) and cylindrical (Igra and Takayama, 2003) gas–liquid (slow–fast) interfaces. In the planar geometry they observed a sequence of three refraction patterns that can be recognized (see Table 2) as RRR, FPR, and FNR, in the Abd-El-Fattah and Henderson (1978b) classification scheme

Table 1
Refraction pattern sequences in gas–gas systems according to the experiments of (Abd-El-Fattah et al. (1976), Abd-El-Fattah and Henderson (1978a) and Abd-El-Fattah and Henderson, 1978b). All patterns could be reproduced in our simulations. Those shown in bold were numerically simulated for the first time in the present paper

$\rightarrow \beta \rightarrow$		
Slow-Fast, Gas-Gas (CO₂/CH₄) Interface:		
\downarrow M_{sh} \downarrow	<i>Very Weak:</i> <i>Weak:</i> <i>Strong:</i>	<i>RRE</i> \Rightarrow <i>RRR</i> \Rightarrow <i>BPR</i> \Rightarrow <i>FPR</i> \Rightarrow <i>FNR</i> <i>RRE</i> \Rightarrow <i>RRR</i> \Rightarrow <i>BPR</i> \Rightarrow <i>FNR</i> \Rightarrow <i>TRR</i> \Rightarrow <i>TNR</i> <i>RRE</i> \Rightarrow <i>BPR</i> \Rightarrow <i>TMR</i>
Fast-Slow, Gas-Gas (Air/SF₆) Interface:		
\downarrow M_{sh} \downarrow	<i>Very Weak:</i> <i>Weak, Strong and Stronger:</i>	<i>RRR</i> \Rightarrow <i>RRE</i> \Rightarrow <i>CFR</i>(<i>ARE</i>) <i>RRR</i> \Rightarrow <i>MRR</i> \Rightarrow <i>CFR</i>
The following notation is used: <i>RRR:</i> Regular Refraction with Reflected shock <i>RRE:</i> Regular Refraction with Reflected Expansion <i>BPR:</i> Bound Precursor Refraction <i>FPR:</i> Free Precursor Refraction <i>FNR:</i> Free precursor von Neumann Refraction <i>TRR:</i> Twin Regular Reflection <i>TNR:</i> Twin von Neumann Reflection <i>CFR:</i> Concave-Forwards irregular Refraction <i>ARE:</i> Anomalous Refraction with reflected Expansion		

Table 2

Listing of known refraction pattern sequences for gas–liquid systems. In the slow–fast case, the patterns are based on our interpretation of Takayama’s experimental images (Takayama, 1987). The definitions are in line with those for gas–gas systems. All these patterns were simulated for the first time in this work. For the fast–slow case, the patterns shown are predictions based on our numerical results and those of Grove and Menikoff (1990)

$\rightarrow \beta \rightarrow$					
Slow-Fast, Gas-Liquid Interface:					
M_{sh} ↓	<table border="0" style="width: 100%;"> <tr> <td style="border-right: 1px solid black; padding: 5px;"><i>Very Weak:</i></td> <td style="padding: 5px;">RRR \Rightarrow FPR \Rightarrow FNR</td> </tr> <tr> <td style="border-right: 1px solid black; padding: 5px;"><i>Weak, Strong and Very Strong:</i></td> <td style="padding: 5px;">...yet to be addressed...</td> </tr> </table>	<i>Very Weak:</i>	RRR \Rightarrow FPR \Rightarrow FNR	<i>Weak, Strong and Very Strong:</i>	...yet to be addressed...
<i>Very Weak:</i>	RRR \Rightarrow FPR \Rightarrow FNR				
<i>Weak, Strong and Very Strong:</i>	...yet to be addressed...				
Fast-Slow, Liquid-Gas Interface:					
<i>Only strong shocks possible</i>	RRE \Rightarrow CFR(ARE)				

(note that the BPR is missing). In the cylindrical geometry the focus was on observing the processes of interface deformation, displacements and accelerations. For the fast–slow case we have Bourne and Field (1992) who employed high-speed photography to visualize shock-induced bubble collapse in a neatly conceived 2D geometry. The focus here was on hypervelocity jet formation, impact on opposite boundaries, and associated light emission.

The main theoretical development is based on the exact analysis by von Neumann (1943) for single node (regular) refraction, which in fact predated even Jahn’s (1956) experiments. The more directly applicable (to interpretation of experiments) generalized von Neumann theory, and the approximate one by Whitham (1958, 1959), followed soon thereafter. Whitham attempts to go beyond regular refractions, and several subsequent extensions (Catherasoo and Sturtevant, 1983; Schwendeman, 1988) were shown to fall short of an adequate description of the reflected wave, as needed for yielding the full refraction pattern spectrum. Nearly 30 years later the subject began to yield to direct numerical simulations.

Henderson et al. (1991) employed an unsteady, two-dimensional, second-order-accurate finite-difference Godunov-based method for perfect gases, using Colella et al. (1989) front-capturing, volume-of-fluid-based method for description of the interface. They considered shock refraction at an initially flat, slow–fast, gas–gas interface (see Table 1), and the results were found to be consistent with Abd-El-Fattah and Henderson’s (1978b) experiments. Grove and Menikoff (1990) considered fast–slow, liquid–gas interfaces and studied “anomalous reflection”, a “pattern” very similar to Abd-El-Fattah and Henderson’s CFR(ARE), in shock-induced bubble collapse and underwater explosion problems. This work was based on a front-tracking method developed by Chern et al. (1985). Lastly, we have Liu et al. (2001), whose aim was to generally demonstrate capabilities of their level-set-based method, to capture interfaces. They presented results for shock-induced bubble collapse and underwater explosion problems, both in the fast–slow configuration. We could not find numerical studies of shock interactions with slow–fast, gas–liquid interfaces.

Besides an interest in completing the picture (see Tables 1 and 2) and in developing a deeper and more comprehensive understanding of the physics involved, the present work is motivated by a broader view of refraction as a canonical problem in compressible multi-hydrodynamics. Specifically, our ultimate objective is to derive a basic understanding and exploit the solutions towards

constructing efficient and accurate numerical schemes for multi-dimensional flow situations which involve shock-interface interactions. In this respect, the proposed path follows naturally from the idea of Godunov (1959) and works of his followers (van Leer, 1979) over the past half century, who have made use of exact and approximate solutions of the one-dimensional Riemann problem for numerical scheme construction. This leads to a dimension-by-dimension treatment, which has been, and remains, seemingly an inescapable approach for treating multi-dimensional problems, with its recognized resolution requirements and potential pitfalls. In contrast, our vision here is for direct tackling of the Riemann problem in a multi-dimensional setting, when a pressure discontinuity (shock plane) and a density discontinuity (e.g., interface) are not aligned. The idea is to apply insights and knowledge about flow patterns emerged from highly resolved and specialized calculations (such as the ones presented in this paper) to provide a better, physics-based treatment of mass, momentum and energy fluxes in general purpose simulations.

This concern is particularly serious for slow–fast, gas–liquid interfaces, for which as Table 2 shows current knowledge is limited to just few experiments. Our experience suggests that for stiff systems (high acoustic impedance mismatch), slow–fast interfaces are much less “forgiving”, and that at the root of this difficulty is the loss of self-similarity, as exhibited under conditions that yield irregular refractions.

As indicated in Tables 1 and 2, in this paper we address all patterns found experimentally in the comprehensive study of Abd-El-Fattah and Henderson for gas–gas systems, and all patterns found experimentally by Takayama for the Very Weak sub-class of slow–fast, gas–liquid systems. In addition we examine the fast–slow, liquid–gas system for which information can be obliquely inferred from the numerical work of Grove and Menikoff (1990) made in the context of shock-induced bubble collapse, and underwater explosion. The so-derived understanding, and scoping calculations lead us to believe that in the slow–fast, gas–liquid system, further rich behavior exists under weak, strong, and extremely strong shocking, a comprehensive consideration of which we leave for future work.

2. Numerical approach

This work was made possible by the recently developed “*Adaptive Characteristics-based Matching*” (aCBM) method (Nourgaliev et al., 2004c, 2005a). In the core of the aCBM is the Structured Adaptive Mesh Refinement (SAMR) methodology, originally developed by Berger and co-authors (Berger and Colella, 1989; Berger and Oliger, 1984; Berger and Rigoutsos, 1991), and implemented as the SAMRAI package in Lawrence Livermore National Laboratory (Wissink et al., 2004). SAMR is based on a sequence of nested, logically rectangular meshes, organized in a hierarchy of $k = 0, \dots, L - 1$ grid levels $\Omega^{h_0} \supset \Omega^{h_1} \supset \dots \supset \Omega^{h_{L-1}}$, where the coarsest grid Ω^{h_0} covers the entire computational domain. Grids are refined in both time and space, with mesh spacings $\underline{h}_k = \{h_0, h_1, \dots, h_k\} |_{k=0, \dots, L-1}$ subject to $h_{k+1} \leq h_k$, and using the same ratio $r = \frac{h_k}{h_{k+1}}$ for refinement in time-space, i.e. $\frac{\Delta t_0}{h_0} = \frac{\Delta t_1}{h_1} = \dots = \frac{\Delta t_{L-1}}{h_{L-1}}$. Thus, the same explicit difference scheme is stable on all levels. As a consequence, more time steps are taken on the finer grids than on the coarser grids, but the smallest time step of the finest level is not imposed globally.

Each level Ω^{h_k} consists of a union of $(M_k + 1)$ logically rectangular regions, or patches, $\mathcal{G}_{k,m} |_{m=0, \dots, M_k}$, at the same grid resolution h_k . The requirement on the numerical algorithm is that

the solution, lying perhaps on multiple patches, is the same. The solution vector $U(\mathbf{x})$ is taken from the finest level. Fig. 6 shows an example of a hierarchy of SAMR grids with three levels of adaptation. A sample of the typical SAMR mesh used in the present study is shown in Fig. 13c.

Time update of a solution on a hierarchy is organized in such a way, as to proceed sequentially from the coarser to finer grids. More specifically, before updating at any level, the next-coarser level solution must be already available, so as to allow the complete inter-level communications needed for populating each patch's ghost cells by interpolation in both time and space. For parallelization, all patches of a hierarchy are distributed between different processors.

The Characteristics-based Matching (CBM) method on uniform meshes was introduced in Nourgaliev et al. (2003, 2004a,b,c). There are three areas where incorporation of the CBM into SAMR (aCBM) required further developments: *inter-patch communication*, *generation/disposal of patches*, and *time update on a patch* (Nourgaliev et al., 2005a).

Inter-patch communication is necessary for synchronization of time updates on different patches. More specifically, it is required to properly populate ghost cells around each patch, before one may proceed with its update. There are three types of inter-patch communications: same-level, coarse-to-fine and fine-to-coarse. The utilities for these operations are provided by SAMRAI, however, in the case of gas–liquid interfaces, the conservative coarse-to-fine and fine-to-coarse inter-level communications fail and needed to be modified. The problem was addressed by means of non-conservative prolongation/restriction operators for specific use in the immediate vicinity of the interface.

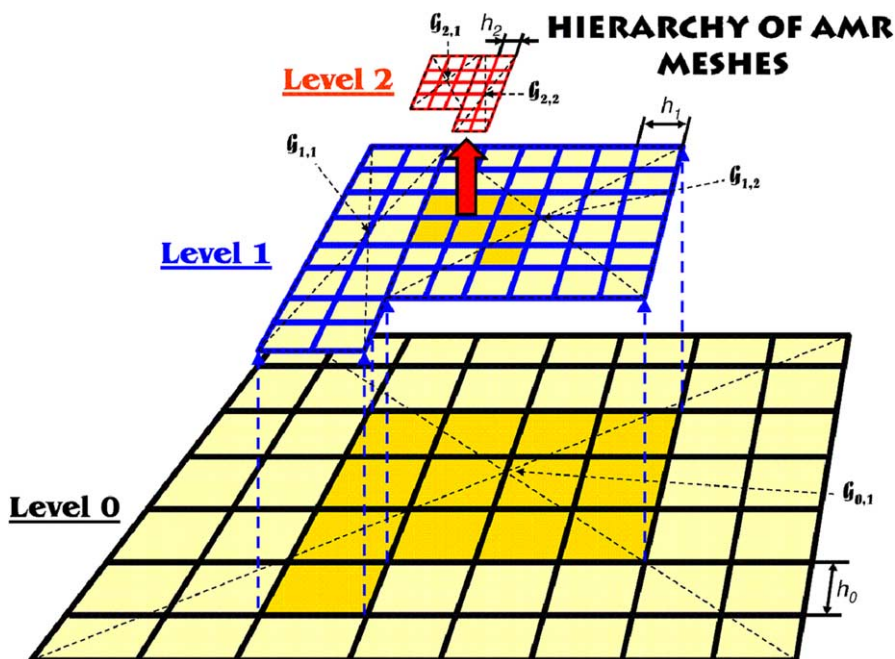


Fig. 6. Sample hierarchy of SAMR meshes.

The second need is related to *adaptive generation/disposal of AMR patches* on different levels of a hierarchy. The SAMR grid may be modified at discrete times. The finest level needs to be changed most often (patches are moved, added or deleted, if required). When the level Ω^{L_k} is changed, all finer levels $\Omega^{L_j}|_{j>k}$ are changed as well, but the coarser levels $\Omega^{L_i}|_{i<k}$ may remain the same. The utilities for dynamic management of AMR patches require tagging criteria for refinement. In the case of compressible multi-phase flows, the computational mesh needs to be refined around flow discontinuities, such as shocks and contacts, as well as around multi-material interfaces. For interfaces we use a distance-based criterium, and for shocks we have a shock-detection criterium that leaves out rarefactions.

Lastly, the major components of our *patch time update strategy* include (a) the third-order-accurate finite-difference method, using the RK₃-TVD scheme for time discretization, the MUSCL₃ scheme (van Leer, 1979) with van Albada's limiter for spatial discretization, and the Local-Lax–Friedrichs (LLF) flux treatment (Nourgaliev et al., 2004b); (b) level-set-based sharp capturing of interfaces, supplemented by localization (FLLS) (implemented by means of a Linear WENO₇ scheme) and WENO₅-based re-initialization algorithms (Peng et al., 1999); and (c) the “characteristics-based matching (CBM)” for coupling solutions across the interface (Nourgaliev et al., 2004b,c). High order discretization and the Linear WENO provide significant benefits in mass conservation of the level set, especially in maintaining under-resolved filamentary structures (Nourgaliev et al., 2005b). The key features of the CBM are (i) a Riemann-solver-based coupling, which is essential for robustness in the case of high acoustic impedance mismatch (i.e., gas–liquid) interfaces, and for accuracy in the case of very strong shock waves in both multi-gaseous and gas–liquid media; and (ii) elimination of the need for ghost fields and corresponding ghost cells; this we found to be necessary for compatibility with AMR. The CBM is based on the generation/tracking/disposal of the subcell-interface-markers (denoted as CBM points), which exist on each patch only during one time step Δt_k . Applying the two-fluid, pseudo-multi-dimensional Riemann solver at CBM points, the wave structure and gas dynamics solutions at the interface are computed and applied for direct modification of numerical fluxes in the Eulerian cells near the interface. This is based on the subcell position of the interface and a flux inter-/extrapolation algorithm. The concept of subcell markers and two-fluid Riemann solutions are borrowed from front-tracking methods (Cocchi and Saurel, 1997). The natural-neighbor interpolation (NNI) procedure is used to correct the numerical solutions at Eulerian computational cells which have found themselves to change fluid occupancy (based on cell center) during the time step. These cells are denoted here as “degenerate” cells. The correction of numerical fluxes and treatment of “degenerate” cells are the substitutes for GFM's (Fedkiw et al., 1999) ghost fields/cells, and the related to them PDE- or FM-based extrapolation techniques.

3. Problem formulation

Following previous studies (Henderson et al., 1991; Grove and Menikoff, 1990), the gas dynamics is described using the two-dimensional Euler equations (Landau and Lifschitz, 1988) neglecting surface tension, viscous and heat transport effects. Numerical simulations were performed using a computational domain of size $L \times H$, see Fig. 7. We set non-reflection boundary conditions at the left, right and top boundaries of the domain, and a symmetry at a bottom boundary.

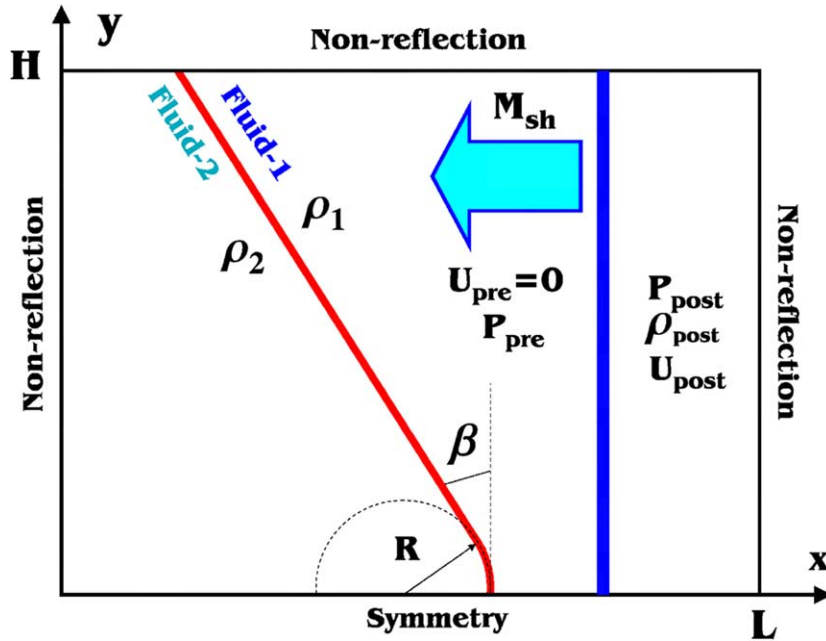


Fig. 7. Definitions used in the numerical simulations.

The interface is specified as shown in Fig. 7, inclined on angle β , with a transition region of curvature $R = \frac{H}{10}$ near the lower boundary. Zero level set separates the computational domain on “positive” and “negative” fluids, both being initially motionless and under pre-shock pressure conditions P_{pre} . Gases are modeled using the ideal-gas-law. Liquids are represented with a stiffened gas equation of state (Nourgaliev et al., 2005a):

$$P = (\gamma - 1)\rho i - P_0; \quad P_0 = \gamma \Pi \tag{1}$$

Pre-shock densities are specified using isothermal conditions. For gas–gas interfaces, we set them by $\rho_2 = \rho_1 \frac{\mu_2}{\mu_1}$, where ρ and μ are density and molecular weight, correspondingly. An incident, i-shock wave of a prescribed strength (characterized by the M_{sh} for gases and/or pressure ratio $\chi_i = \frac{P_{pre}}{P_{post}}$ for liquids) is placed in Fluid-1, as depicted in Fig. 7. After impact upon the interface, the i-shock is refracted. Numerical results are displayed as fields of pressure, numerical Schlieren and Mach number. The numerical Schlieren fields are generated in the manner described by Quirk and Karni (1996), with the following nonlinear shading function ϑ :

$$\vartheta = \exp \left(-\kappa \frac{|\nabla \rho|}{|\nabla \rho|_{max}} \right) \tag{2}$$

The accentuation coefficients κ chosen were problem-specific.

The computational domain is discretized with a grid resolution of $\Delta x = \Delta y = \frac{H}{50}$ on the coarsest AMR level. Using 3 levels of AMR adaptation with refinement ratio 4, the effective resolution on the finest AMR level was $\Delta x = \Delta y = \frac{H}{800}$.

4. Slow–fast, gas–gas interface

Here we simulate shock refraction at a CO_2/CH_4 interface, as utilized in the Abd-El-Fattah and Henderson's (1978b) experiments. The gases are represented by the following ratios of specific heats and molecular weights: $\gamma_{\text{CO}_2} = 1.288$, $\gamma_{\text{CH}_4} = 1.303$, $\mu_{\text{CO}_2} = 44.01$ and $\mu_{\text{CH}_4} = 16.04$. Following previous numerical studies (Henderson et al., 1991), the effects of the membrane used to separate initially the gases are neglected. Simulations were performed varying the angle of the attack β for incident shock strengths corresponding to the *Very Weak* ($M_{\text{sh}} = 1.12$ and $\chi_i = 0.78$), *Weak* ($M_{\text{sh}} = 1.34$ and $\chi_i = 0.53$), and *Strong* shock ($M_{\text{sh}} = 2.25$ and $\chi_i = 0.18$) sequences in the experiments. Comparisons are made in two ways: (a) directly with experimental images, which are legible enough only in a followup (the simulation) paper (Henderson et al., 1991), and only for the selected cases of FNR (Very Weak), TRR and TNR (Weak) and TMR (Strong), and (b) indirectly, by using the definitions and maps of Abd-El-Fattah and Henderson (1978b) for all cases shown in Table 1, since the experimental images are not of sufficient clarity in the original publications.

All patterns in Table 1 for the Very Weak sequence were reproduced quantitatively in the simulations. The following discussion of main trends is given with the help of the sample results in Figs. 8 and 9, and a shock polar analysis based on the generalized von Neumann theory. For angles of the attack below $\beta_i = 32.0592^\circ$, the pattern is regular and the reflected wave is an expansion, Fig. 8a. With an increase of β , the reflected expansion wave becomes weaker. At the angle of *intromission* β_i , the reflection is reduced to a *Mach line degeneracy*. In a shock polar diagram (Fig. 8b, right), this corresponds to the point where the incident shock, transmitted shock and reflected shock/expansion polars intersect at one point. At these conditions, the incident shock wave is totally transmitted. With a further increase of β , the reflected wave becomes a shock, Fig. 8c. In the range of $\beta_i < \beta_{\text{sc}}$, there are two solutions of the von Neumann's theory (known as weak and strong shocks) - corresponding to two possible deflection angles. The weak solution, shown in Fig. 8c (right), was observed in the experiments. This is also the solution which is obtained in our numerical simulations. At the *shock critical angle* $\beta_{\text{sc}} = 34.4885^\circ$, weak and strong solutions collapse into one, Fig. 8d (right). With a further increase of β , there are no solutions according to a shock polar analysis, and the refraction pattern becomes *irregular*.

There are three irregular refraction patterns observed in the experiments as well as in our simulations. The first one, called *Bound Precursor Refraction* (BPR), is shown in Fig. 9a. In this pattern, even though the transmitted, t-shock is always ahead of the i-shock, it moves along the interface at nearly the same velocity. The major difference of the BPR from the RRR is in the appearance of a fourth wave and the fact that the t-wave leans forward, instead of leaning-backwards, as seen in the RRR pattern (and as noted by Henderson et al., 1991).

As the angle β is further increased, the BPR pattern transforms into the *Free Precursor Refraction* (FPR), see Fig. 9b. In it the t-wave breaks loose from the i- and r-shocks, running significantly ahead along the interface. It is also locally smeared out, transforming into a so-called *evanescent wave* (Henderson et al., 1991), which is refracted back from the CH_4 into the CO_2 as a side, s-wave. This secondary refraction is of the fast–slow type. The s-wave is also evanescent. There are no signs for reflection of the t-wave, which is consistent with the experiments and the Henderson et al. (1991) simulations. Presumably, these reflected waves are too weak to be visible

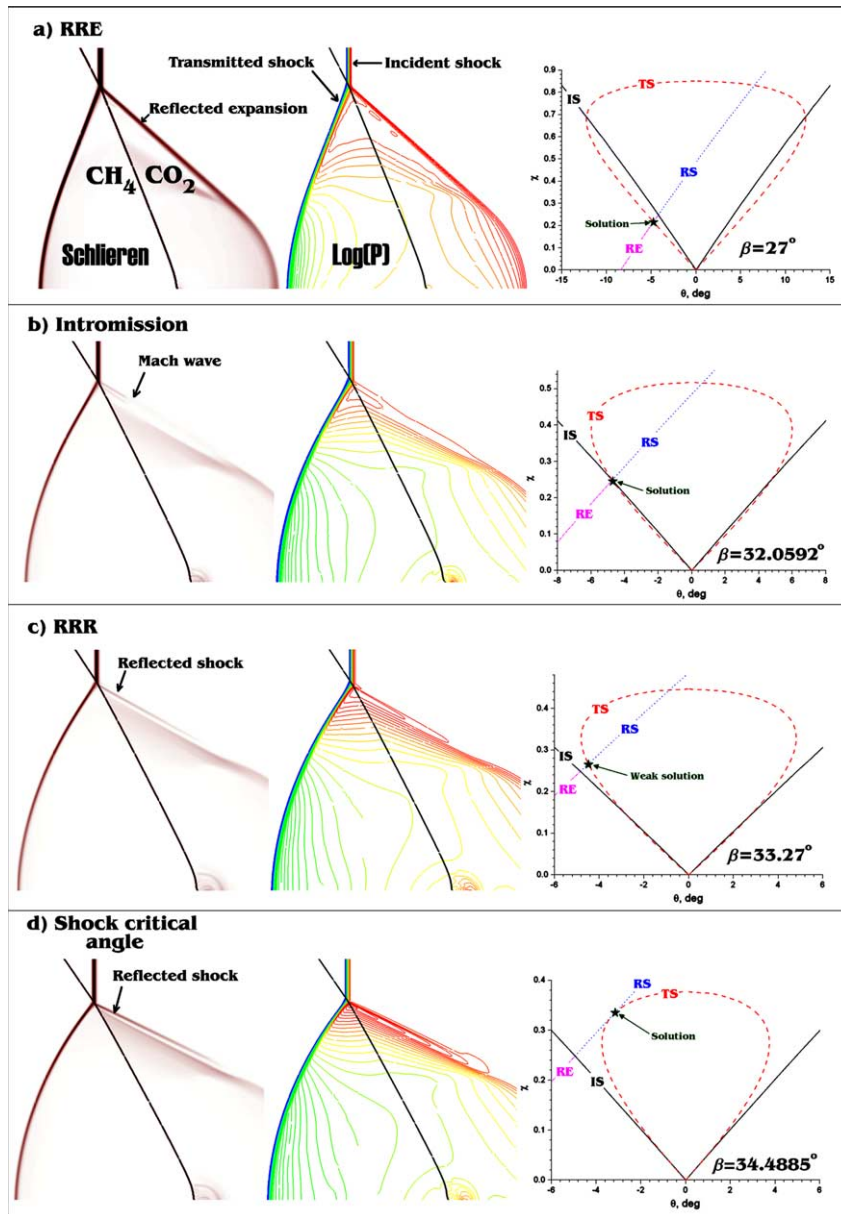


Fig. 8. Regular refraction at slow–fast, gas–gas interfaces. Very Weak shock sequence ($\chi_i = 0.78$). Left: numerical Schlieren; center: $\log P$; right: pressure–deflection (or shock–polar) diagram (PDD). Notation used in PDDs: IS—incident shock polar; TS—transmitted shock polar; RS—reflected shock polar and RE—reflected expansion curve.

in pressure contour plots. The s-wave interacts with the i-wave, modifying it into a k-wave, which in turn is reflected as a centered expansion e-wave. The e-wave interacts with the reflected shock r-wave, causing almost complete mutual annihilation.

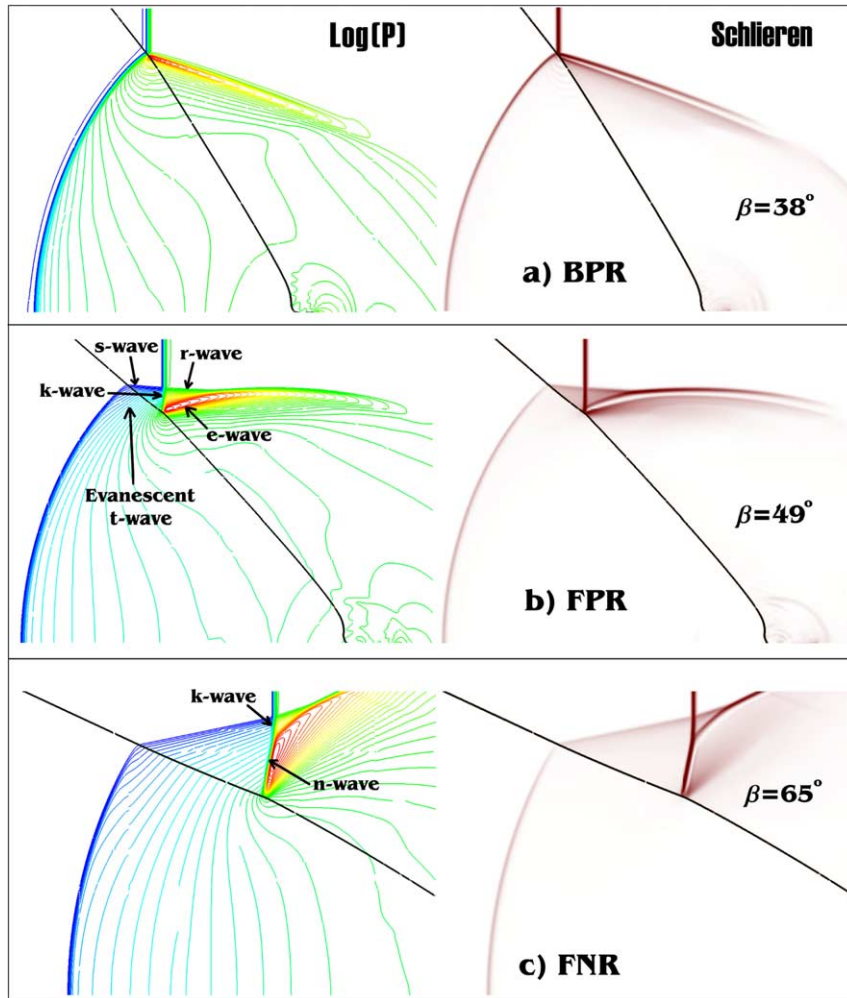


Fig. 9. Irregular refraction at a slow-fast, gas-gas interface. Very Weak shock sequence ($\chi_i = 0.78$).

Under even higher angle β , the FPR undergoes a further transition to another pattern, called a *Free precursor von Neumann Refraction* (FNR), shown in Fig. 9c. It is characterized by a formation of a weak Mach reflection, denoted in Fig. 9c as n-wave.

As discussed by Henderson et al. (1991), the transition from one pattern to another is sensitive to the numerical treatment and grid resolution. Our simulations, performed with 2° increments of β , indicate that the CBM interface boundary condition capturing, together with the AMR are capable to accurately describe these transitions.

The Strong sequence in Table 1 was also reproduced quantitatively in the simulations. Now there are only three patterns, a sampling of which can be seen in Fig. 10. In comparison to the Very Weak sequence the RRR and FPR are absent, and the TMR is new. In contrast to the FPR pattern of the Weak shock series, the t- and s-waves of the TMR are not evanescent

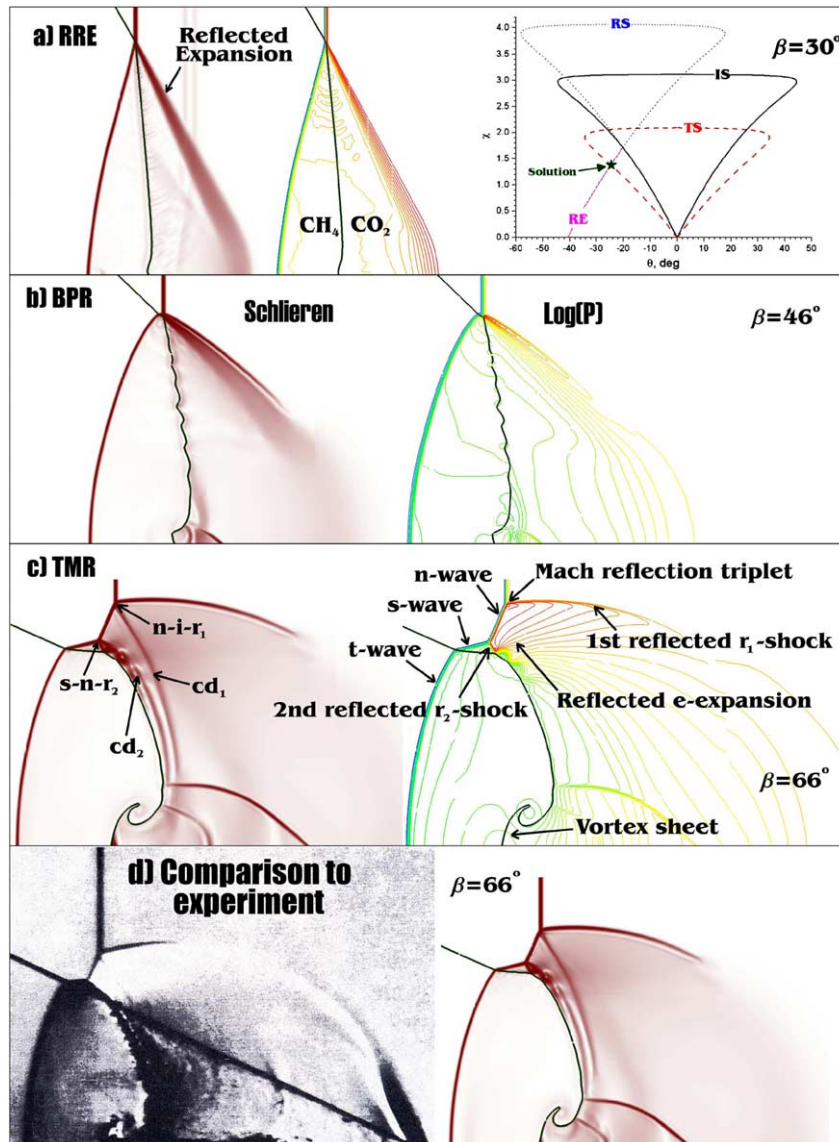


Fig. 10. (a–c) Refraction patterns at a slow–fast, gas–gas interface. Strong shock sequence ($\chi_i = 0.18$). (d) On the left is the Schlieren from the experiment.

compressions. Interaction of the s-wave with the incident shock results in a formation of two Mach reflection triplets, shown as s- r_2 -n and n-i- r_1 systems in Fig. 10c. The reflected shock is split into two waves, denoted as r_1 and r_2 . There are two contact discontinuities, originated from each of the Mach stems, shown as cd_1 and cd_2 in Fig. 10c. Notably, as the second contact passes through the reflected expansion e-wave, it becomes unstable, due to the misalignment of pressure and density gradients (Richtmyer–Meshkov instability). Direct comparison to the only legible

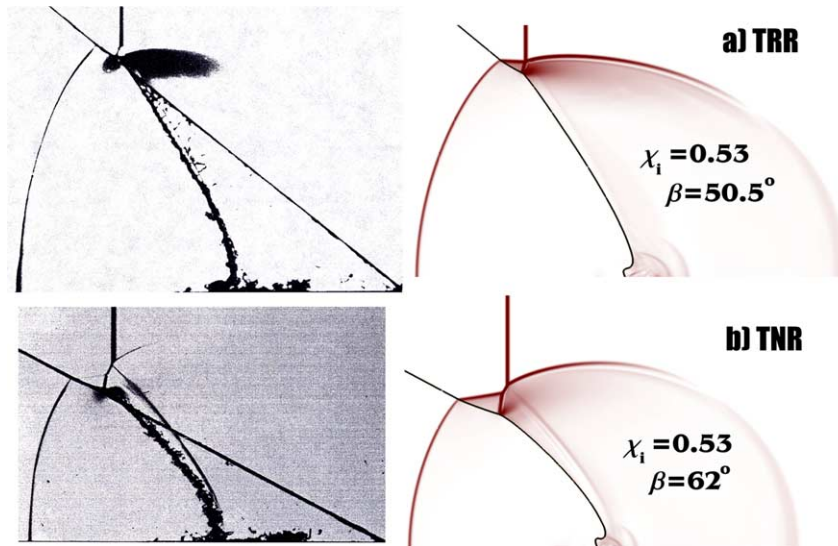


Fig. 11. Refraction patterns at a slow-fast, gas-gas (CO_2/CH_4) interface for the Weak shock sequence. On the left are the Schlieren images from the experiment.

experimental image, the TMR, for this sequence is given in Fig. 10d. Note that the second predicted contact, cd_2 , is not visible in the experiment, probably due to the poor quality of the image.

Similarly good simulations were obtained for the Weak sequence. As shown in Table 1, in comparison to the Very Weak case, we see the appearance of two new patterns, the TRR and the TNR, shown in Fig. 11, which also includes a direct comparison with the experiments. These two patterns can be conceptually described as a transition from the Very Weak shock's FNR to the Strong shock's TMR patterns. More specifically, with the increase of the shock strength, the back-transmitted s-wave (Fig. 9c) becomes strong enough to interfere with the incident shock, forming a four-shock TRR pattern. Next, with further increase of the shock strength, the four-shock is split into two Mach reflections, very similar to the TMR, but named as twin von Neumann reflection TNR in the experimental paper (Abd-El-Fattah and Henderson, 1978b).

Fig. 12 presents wave deflection angles, obtained in our simulations, with comparison to those from the experiment (Abd-El-Fattah and Henderson, 1978b). As one can see, there is excellent agreement for deflections of interface δ_i and reflected wave α_r . Our transmitted shock angle α_t begins to diverge from the experimental data at $\beta \sim 30^\circ$, and the deviation reaches $\sim 20^\circ$ at the upper end of the range. A similar trend was found by Henderson et al. (1991), who ignored, as we did, the gas interdiffusion (limited initial smearing of the interface) that was reportedly observed in the experiments.

4.1. Grid convergence studies

The effect of grid resolution on capturing of regular refraction patterns is demonstrated in Fig. 13. We use three grids, with 1, 2 and 3 levels of AMR adaptation, and refinement ratio 4, corresponding to effective grid resolutions on the finest AMR level $\Delta x = \frac{H}{50}$, $\frac{H}{200}$ and $\frac{H}{800}$,

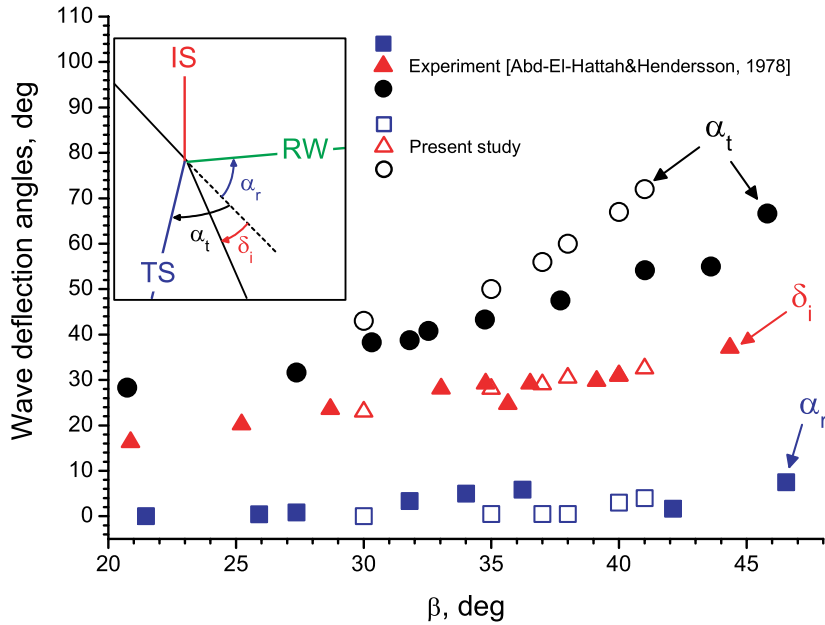


Fig. 12. Comparison of numerical and experimental results for wave deflection angles in the refraction of a strong $\chi_i = 0.18$ plane shock wave at CO_2/CH_4 interface.

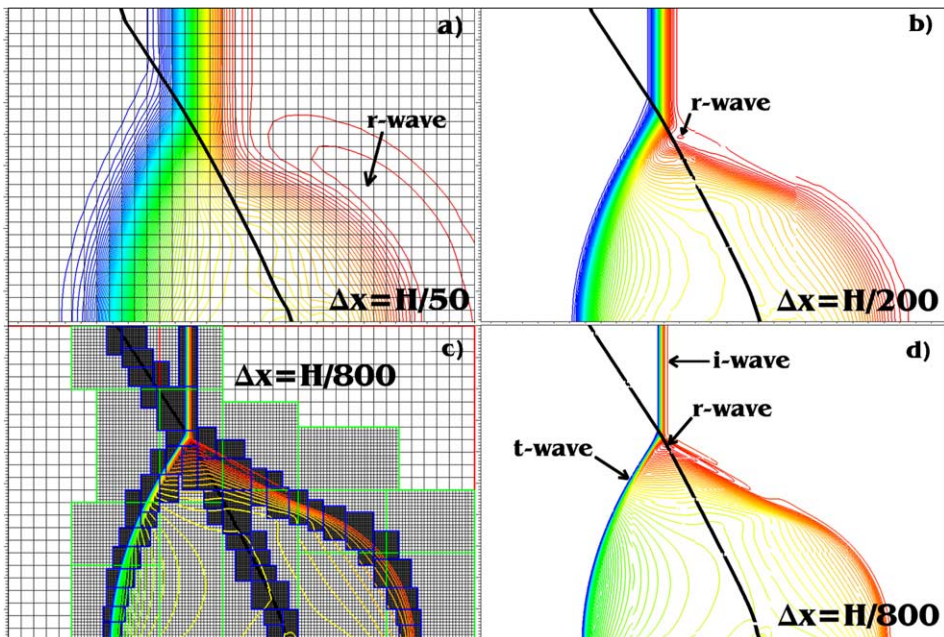


Fig. 13. The effect of under-resolution for a regular refraction pattern. CO_2/CH_4 interface under $\chi_i = 0.78$. Pressure field ($\log P$) and position of the interface for $\beta = 33.27^\circ$.

respectively. A typical mesh with three levels of adaptation is shown in Fig. 13c. As one can see in these results, for the regular, RRR pattern, the overall λ -structure is captured well even on a coarse grid. The reflected r-wave is properly predicted as a shock. The effect of the under-resolution is

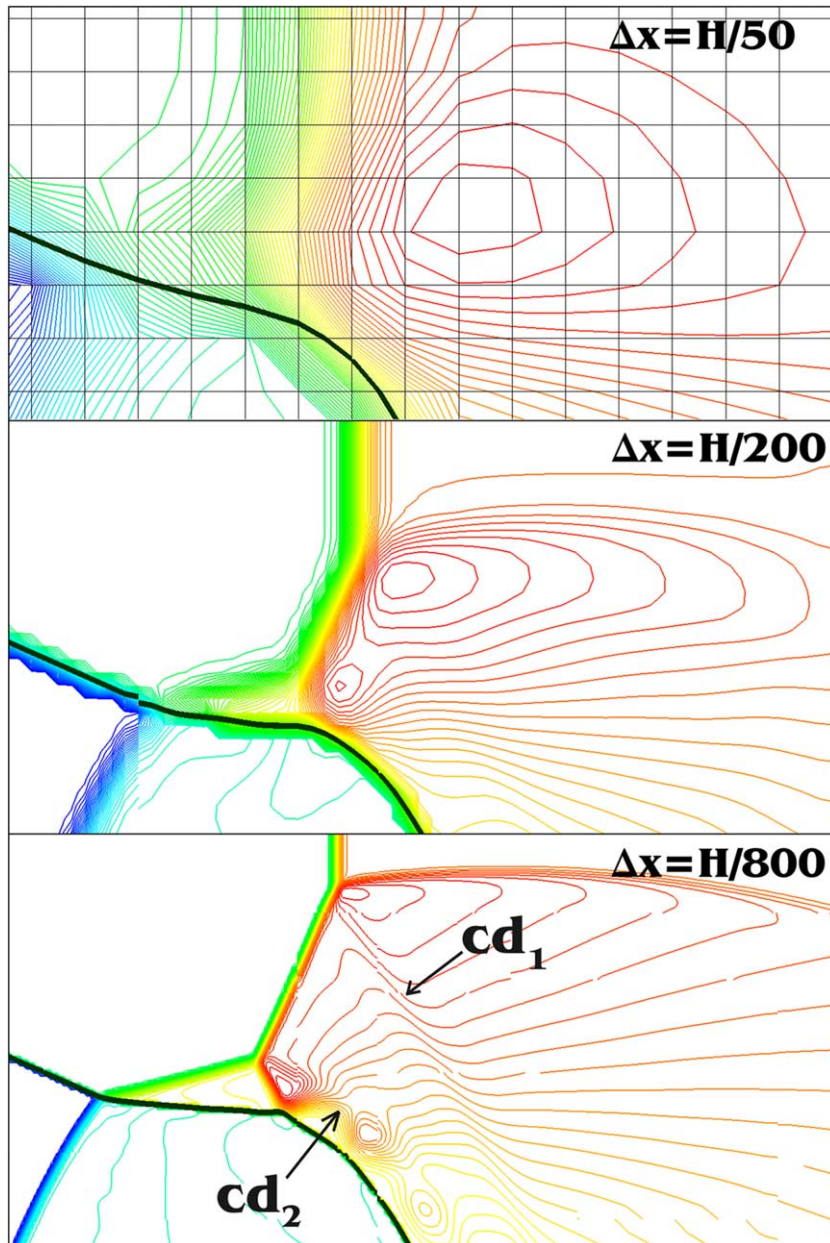


Fig. 14. The effect of under-resolution for an irregular TMR refraction pattern. CO_2/CH_4 interface under $\chi_i = 0.18$. Density field and position of the interface for $\beta = 66^\circ$.

that the position of the r-wave is displaced from the refraction node, Fig. 13a. As the grid is sequentially refined, the solution converges to a proper position of the r-wave, i.e., stemming from the refraction node.

On the other hand, in the case of irregular refraction, such as the TMR shown in Fig. 14, the effect of under-resolution is dramatic. Under the coarsest grid, $\Delta x = \frac{H}{50}$, the complex double-Mach reflection structure is completely lost. Under the intermediate grid, $\Delta x = \frac{H}{200}$, the twin Mach reflections start to emerge, however, the grid resolution is still not adequate enough to capture the formation of contact discontinuities cd_1 and cd_2 , which can only be seen on the finest grid, $\Delta x = \frac{H}{800}$.

5. Fast–slow, gas–gas interface

This category is represented by the Air/SF₆ experiments of Abd-El-Fattah and Henderson (1978a) (see Table 1). The gases are modeled with the following ratios of specific heats and molecular weights: $\gamma_{\text{Air}} = 1.4$, $\gamma_{\text{SF}_6} = 1.08$, $\mu_{\text{Air}} = 29.02$ and $\mu_{\text{SF}_6} = 130.071$. Three series of simulations were carried out, corresponding to *Very Weak* ($\chi_i = 0.85$), *Weak* ($\chi_i = 0.66$), and *Strong shock sequences* ($\chi_i = 0.25$). There are no previous simulations of these experiments, and the images available are not of a sufficient quality for direct comparisons. Resorting to indirect comparison, using the definitions, and maps of Abd-El-Fattah and Henderson (1978a), we found the agreement to be excellent over the whole spectrum of conditions and patterns (Table 1). As seen in this table, the sequence of patterns in Weak, Strong and Stronger, are essentially the same, and so are they in our simulations.

The Very Weak sequence consists of three patterns $\text{RRR} \Rightarrow \text{RRE} \Rightarrow \text{CFR}(\text{ARE})$, as illustrated in Fig. 15. The *Concave-Forwards Refraction* (CFR) is an irregular pattern, with reflected expansion

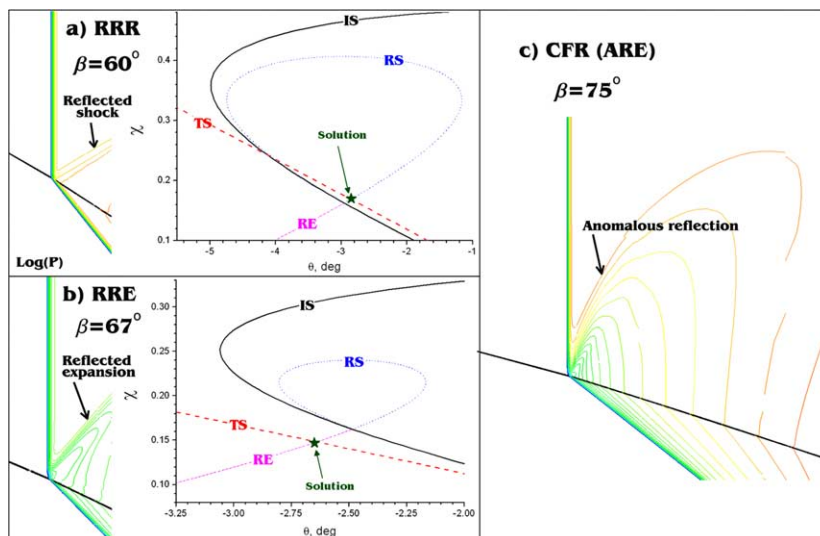


Fig. 15. Sequence of refraction patterns at a fast–slow, gas–gas interface. Very Weak shock sequence ($\chi_i = 0.85$).

sion wave. The incident shock interacts with the reflected wave (marked as anomalous reflection, Fig. 15c) and eventually it becomes curved. This can be more clearly seen in Fig. 19. This pattern is analogous to anomalous reflection (ARE) of Grove and Menikoff (1990), which will be discussed in Section 6.

The Weak sequence begins with a regular pattern, RRR, which, with increasing β , first transforms into the *Mach Reflection–Refraction* (MRR) and then into the CFR already seen above. Sample results are shown in Fig. 16. The MRR exists under a rather narrow range of incident angles here; it is discussed under the Strong sequence in which it is more pronounced (this may be the difference that lead Abd-El-Fattah and Henderson to keep the Weak and Strong (and Stronger) sequences separate, in spite of their apparent similarity, as noted above). In difference to the CFR of the Very Weak sequence, in this case the reflected wave is not expansion, but a band of weak wavelets, which are remnants of disintegrated shock wave of the previous RRR pattern.

Sample results of a Strong sequence are shown in Fig. 17. The Mach Reflection–Refraction (MRR) pattern is now pronounced. It is characterized by the appearance of the Mach reflection, as a triplet of t–i–r waves, Fig. 17b. There is a contact discontinuity cd, which originates from the Mach stem. Passing through the expansion e-wave, it becomes unstable due to a misalignment of the pressure and density gradients (Richtmyer–Meshkov instability). It is very similar to the cd₂-instability in the TMR pattern of the slow–fast interface, discussed in conjunction with Fig. 10c. The generated vortices interact with the interface, making it unstable too. The CFR pattern is similar to the ones found in the Very Weak and Weak sequences, discussed above.

Clearly, for all cases of shock strength the fast–slow configuration is by far less rich in refraction patterns compared to the slow–fast category. This is because the transmitted wave is attached to the interface, without any chance for back-refraction, which is one of the main reason for a great variety of refraction patterns in the slow–fast configuration.

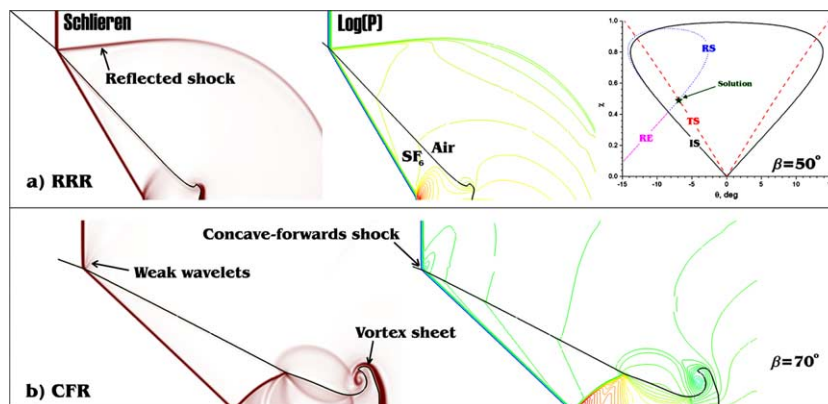


Fig. 16. Samples of refraction patterns at a fast–slow, gas–gas interface (RRR and CFR). Weak shock sequence ($\chi_i = 0.66$).

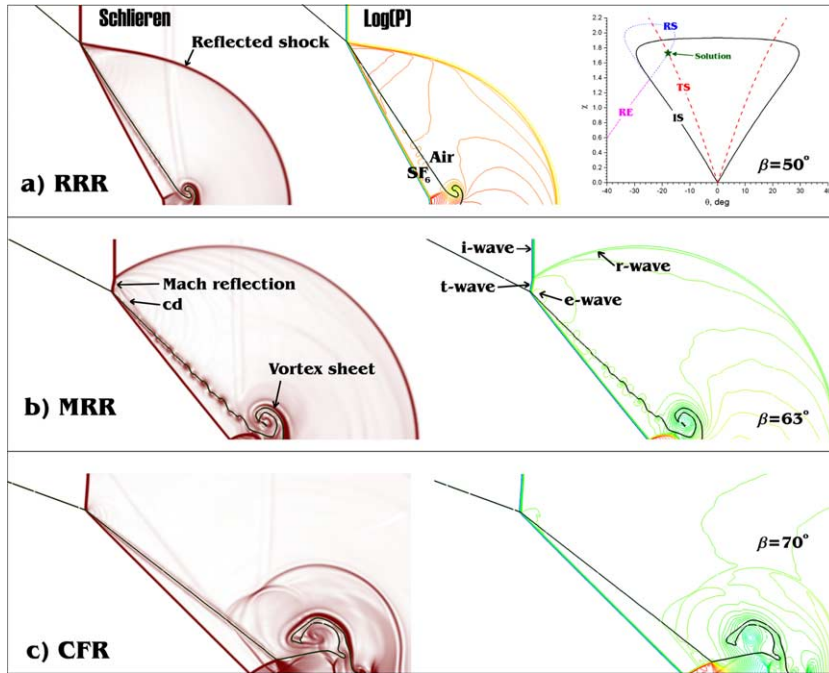


Fig. 17. Sequence of refraction patterns at a fast–slow, gas–gas interface. Strong shock sequence ($\chi_i = 0.25$).

6. The gas–liquid interface

Here we simulate the air–water interface in both the fast–slow and slow–fast configurations. The air is modeled as a perfect gas with $\gamma_{Air} = 1.4$, and for the water we use stiffened gas equation of state with $\begin{bmatrix} \gamma \\ \Pi \end{bmatrix} = \begin{bmatrix} 4.4 \\ 6 \times 10^8 \end{bmatrix}$ and $\begin{bmatrix} 2.8 \\ 3.036 \times 10^8 \end{bmatrix}$ for the high pressure (fast–slow) and low pressure (slow–fast) cases, respectively. In the fast–slow case, relevant previous work is that of Grove and Menikoff (1990) who considered shock-induced bubble collapse and underwater explosion problems. Here the problem makes sense only in the case of Strong shocks (extremely low values of χ). In the slow–fast case, we compare to Takayama’s (1987) data that covered only a Very Weak shock sequence.

6.1. Fast–slow configuration

A strong $M_{sh} = 1.72$ incident shock, $\chi_i = 5.3 \times 10^{-5}$ is placed in water, corresponding to the following pre- and post-shock conditions:

$$V_{pre-shock} = \begin{bmatrix} 1 \times 10^5 \\ 1000 \\ 0 \\ 0 \end{bmatrix} \text{ and } V_{post-shock} = \begin{bmatrix} 1.9 \times 10^9 \\ 1323.65 \\ -681.58 \\ 0 \end{bmatrix},$$

where \mathbf{V} is a vector of primitive variables, $(P, \rho, u, v)^T$, in (Pa, kg/m³, m/s, m/s). As the refraction patterns for this configuration are simple, there is no difficulty in capturing them on rather coarse grids. Numerical simulations were performed using effective grid resolutions of $\Delta x = \frac{H}{800}$, so as to better represent the Mach/pressure fields.

The computational results are shown in Fig. 18, as a sequence for different angles of the attack β . For small β 's, the refraction pattern is regular and of the *RRE-type*. This is different from the gas–gas configuration, where the reflected wave is an expansion **only** for the *Very Weak* case (see Table 1). Represented in a shock polar diagram, the locus of states for an incident shock in a stiff (liquid) media is very tall and narrow, compared to the shock polar for a transmitted shock wave in a gas. Thus, the only way to connect these two is through a reflected expansion curve. Also note that there is no possibility here for reflected shock (RRR), nor can we have the MRR found in gas–gas systems (see Table 1). Rather as the angle of the attack is increased further, an irregular refraction pattern is formed. This refraction is similar to the *CFR* which appears as the terminal pattern for fast–slow, gas–gas interfaces as seen above. It is characterized by a forwards-concave incident shock wave, which runs ahead of the transmitted wave. This type of refraction was seen in calculation of shock-induced bubble collapse, and was named *anomalous reflection* (ARE) by Grove and Menikoff (1990).

The flat interface configuration and high grid resolution used in the present study allows for the more clear presentation of physical mechanisms involved in CFR(ARE). Under a regular refraction, Fig. 19a and b, the r-wave is a centered fan of Prandtl–Meyer expansion waves. The leading edge of the r-wave is inclined on angle α relative to the incident shock, Fig. 19b. As the angle of the attack β increases, the leading edge of the r-wave becomes more and more oblique relative to the incident i-wave. At some β , the r-wave starts to run parallel to the i-wave, $\alpha \rightarrow \alpha_a \approx 0$. At this moment, the causal relationship “incident wave \Rightarrow reflected wave” is violated, the problem becomes non-hyperbolic, and the i-wave starts to interact with the reflected wave, “i-wave \Leftrightarrow r-wave”, which results in a mutual annihilation and formation of a compound (i,r)-wave. The incident shock becomes weaker in a close neighborhood of the refraction node, and, as a result, the speed of the refraction node, defined as intersection of (i,r)- and t-waves, is smaller

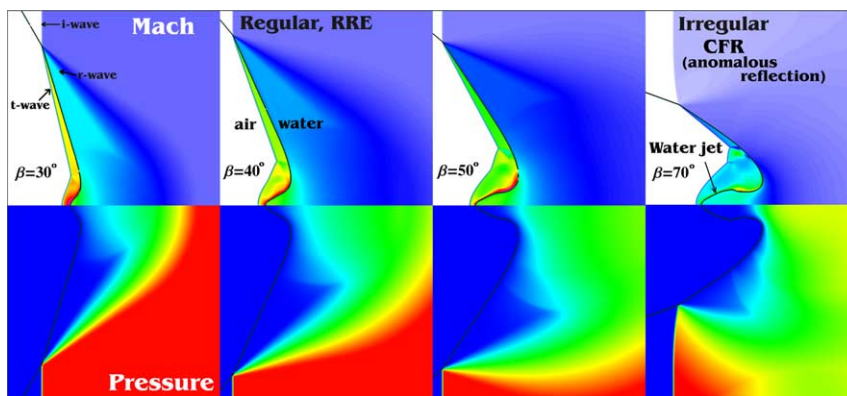


Fig. 18. Shock refraction at a fast–slow, water–air interface. $\chi_i = 5.3 \times 10^{-5}$. Note the water jet beginning to form due to the convergence of shock-induced flows, as predicted by Tulin et al. (1969).

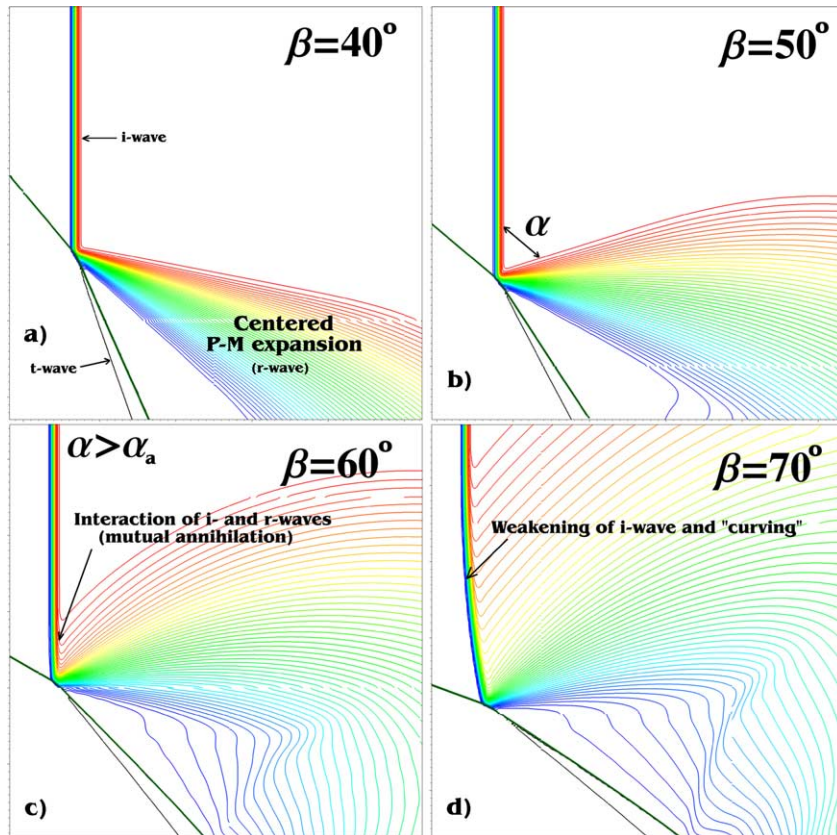


Fig. 19. On physical mechanisms for CFR(ARE) pattern on a fast–slow, water–air interface.

than the speed of the original incident shock *i*-wave. This causes a curving of the compound (*i*, *r*)-wave and a formation of the Concave-Forwards Refraction (CFR) structure. Grove and Menikoff (1990) offered similar explanation for the curving, however, their simulation results were not as clear, especially for the transition RRE \Rightarrow CFR, due to the curvature in the interface itself and low grid resolution.

6.2. Slow–fast configuration

As in the experiments of Takayama (1987), an incident shock of the strength $M_{sh} = 1.47$ is placed in the air. As we have seen in Section 4 this is the case of Very Weak shock in the Abd-El-Fattah and Henderson's classification.

Sample computational results are shown in Fig. 20 revealing the sequence RRR \Rightarrow FPR \Rightarrow FNR. A key differences from the earlier-discussed, slow–fast refractions at gas–gas interfaces is that the post-transmitted state is subsonic and the BPR pattern is absent. Up to a certain angle of attack, $\beta_{cr} \approx 36^\circ$, the combination of the transmitted *t*-pressure wave, incident *i*- and re-

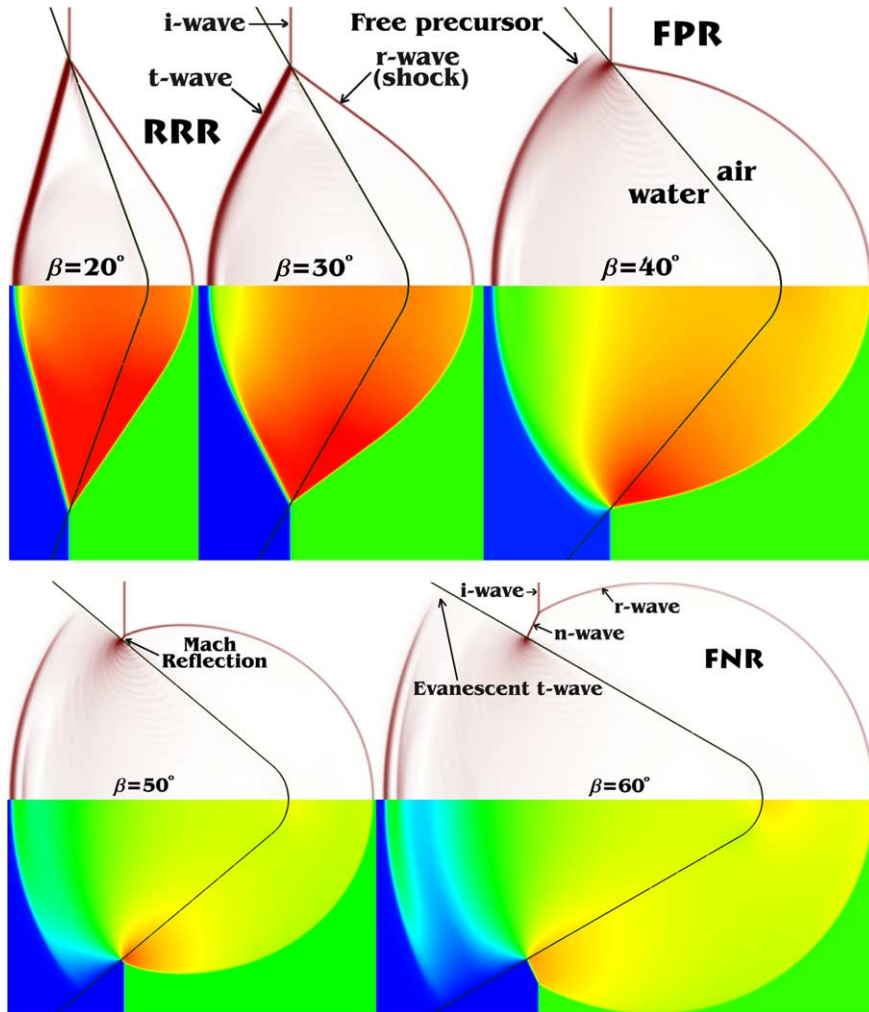


Fig. 20. Shock refraction at a slow-fast, air-water interface. $\chi_i = 0.426$. Top: numerical Schlieren, bottom: $\log_{10} P$.

flected r-shock waves observed corresponds to regular refraction-point pattern (*RRR-type*) and the transmitted shock leans backwards, relative to the interface, as shown in Fig. 21.

At higher β values, the refraction pattern becomes irregular. In a very narrow range around β_{cr} , the t-wave is a precursor and nearly orthogonal to the interface, which is similar to a *BPR pattern* in a gas-gas, slow-fast interface. With a further increase of β , the t-wave gets “loose” and runs away from a refraction point, which we define as the intersection of i- and r-waves. This corresponds to the *FPR pattern* in a gas-gas interface configuration. With our grid resolution of $\Delta x = \frac{H}{800}$, we could detect the transitions $RRR \Rightarrow FPR$, within 1° of accuracy. The important feature of the FPR pattern is that the t-wave leans forwards. The precursor pressure wave is clearly evanescent. The transmitted pressure wave is weak, and no back-refraction of this wave into the air is possible (or observed).

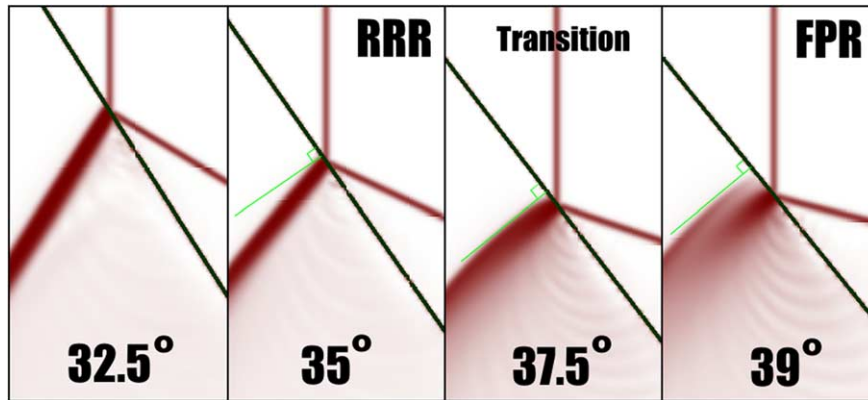


Fig. 21. Details of transition from RRR to FPR for a slow–fast, air–water interface problem. Numerical Schlieren near the critical angle of $\beta_{cr} \approx 37^\circ$.

When the angle of the attack is further increased, a Mach reflection is formed, which can be seen in Fig. 20 for $\beta = 50^\circ$ and 60° . This is very similar to the *FNR* pattern seen for gas–gas interfaces, except for the absence of any significant side wave, capable of interacting with the incident shock.

7. Concluding remarks

Computational results for a slow–fast, gas–gas (CO_2/CH_4) interface reveal eight different refraction patterns, consistent with the von Neumann’s theory for regular refraction, and Abd-El-Fattah and Henderson’s experimental data that systematically covered the whole range of shock strengths and angles of attack. Numerical simulations of shock refraction at fast–slow, gas–gas interfaces, performed for the first time here, exhibit the existence of four basic patterns, i.e., RRR, RRE, MRR and CFR, as observed in the experiments for an air- SF_6 interface by Abd-El-Fattah and Henderson (1978a).

Simulations for the liquid–gas, fast–slow interface, carried out for the first time here for a planar interface, under strong shock conditions, exhibit only two refraction patterns, a regular one, RRE, and an irregular one, CFR(ARE). The RRR and MRR patterns found in gas–gas systems are missing; that is, the reflected wave in liquid–gas systems is always an expansion.

Simulations for the gas–liquid, slow–fast interface, carried out for the first time here, covered the Very Weak incident shock case, as considered in Takayama’s experiments, and results are in excellent agreement with these data. The three patterns found, RRR, FPR, and FNR, are similar to those for gas–gas systems for the Very Weak case, but there are some differences, such as a weak transmitted subsonic pressure wave instead of supersonic transmitted shock waves in a gas–gas systems, and details of the flow structures in the Free von Neumann precursor Refraction. Scoping calculations (not presented here) indicate that as the shock strength increases, additional, complex patterns, not found in gas–gas systems appear, and these will be addressed in future work.

“Simple” patterns are spatially self-similar, so that the basic structure can readily be captured on a rather coarse grid. For such simple patterns, convergence with grid resolution is monotonic, that is no new patterns appear. On the other hand, simulations and analysis show that as the interaction angle increases, complexity emerges in the form of increasingly intricate irregular patterns. An example of a mildly irregular pattern is the CFR, which occurs when the interaction outcome (such as a reflected expansion) interferes with the incident shock, complicating the causal relationship between the cause (shock) and the effect (reflected wave). The non-linearity is manifested strongly in other irregular patterns (e.g., FPR, FNR, TMR, etc.), through a non-local behavior with distinct changes in patterns as one moves outwards from the “origin” (i.e., shock-interface interaction point). We showed that such irregular patterns cannot be captured in simulations on a coarse grid. Things become even more complex for irregular patterns whose structures evolve dynamically in time, necessitating the use of a time scaling in characterizing the pattern structure.

Interestingly, for gas–liquid interfaces, we observe that the pattern in the fast–slow configuration (i.e., shock-induced bubble collapse) remains essentially regular all the way up to high incident angles, even under extremely strong shock conditions. This is to be contrasted with highly irregular patterns, including the run-away precursor shock, which emerge even for relatively low angles (between 30° and 40°) at a slow–fast, gas–liquid interface (i.e., liquid drop subjected to a gaseous shock). We suggest that this difference is the essential cause for the ease and challenge, correspondingly, of numerical simulation involving these two configurations.

Finally, we would like to recall that all computations presented here are performed using dimension-by-dimension treatment of numerical fluxes. With sufficiently high grid resolution, this approach seems to be adequate to describe all refraction patterns at well-developed pattern stages. In many simulations of practical situations however, the patterns are either under-resolved (especially for non-local behaviors discussed above) or under-developed. In these cases, it is important to reflect non-local and dynamic behaviors of the shocked interface directly in the construction of numerical fluxes. The approach being pursued by the present authors is to make use of well-resolved irregular patterns computed by the aCBM method to construct sub-grid-scale models which can guide a proper (multi-dimensional) construction of numerical fluxes, improving performance for under-resolved and under-developed flow structures.

Acknowledgements

This work was supported by the Lawrence Livermore National Laboratory (“ALPHA”, “MIX” and “ASOS” projects), the National Ground Intelligence Center (NGIC), the Defense Threat Reduction Agency (DTRA) and the US Army. Support of Drs. Frank Handler and Glen Nakafuji at LLNL, Dr. Rick Babarsky at NGIC, Ed Conley, JBCCOM at RDEC, and Mr. John Pace and Mr. Charles Fromer of the JSTO at DTRA is gratefully acknowledged.

References

- Abd-El-Fattah, A.M., Henderson, L.H., 1978a. Shock waves at a fast–slow gas interface. *Journal of Fluid Mechanics* 86, 15–32.

- Abd-El-Fattah, A.M., Henderson, L.H., 1978b. Shock waves at a slow–fast gas interface. *Journal of Fluid Mechanics* 89, 79–95.
- Abd-El-Fattah, A.M., Henderson, L.H., Lozzi, A., 1976. Precursor shock waves at a slow–fast gas interface. *Journal of Fluid Mechanics* 76, 157–176.
- Berger, M.J., Colella, P., 1989. Local adaptive mesh refinement for shock hydrodynamics. *Journal of Computational Physics* 82, 67–84.
- Berger, M.J., Olinger, J., 1984. Adaptive mesh refinement for hyperbolic partial differential equations. *Journal of Computational Physics* 53, 482–512.
- Berger, M.J., Rigoutsos, I., 1991. An algorithm for point clustering and grid generation. *IEEE Transactions on Systems, Man, and Cybernetics* 21, 1278–1286.
- Bourne, N.K., Field, J.E., 1992. Shock induced collapse of single cavities in liquids. *Journal of Fluid Mechanics* 244, 225.
- Catherasoo, C.J., Sturtevant, B., 1983. Shock dynamics in non-uniform media. *Journal of Fluid Mechanics* 127, 539–561.
- Chern, I.L., Glimm, J., McBryan, O., Plohr, B., Yaniv, S., 1985. Front tracking for gas dynamics. *Journal of Computational Physics* 62, 83–110.
- Cocchi, J.-P., Saurel, R., 1997. A Riemann problem based method for the resolution of compressible multimaterial flows. *Journal of Computational Physics* 137, 265–298.
- Colella, P., Glaz, H.M., Ferguson, R.E., 1989. Multifluid algorithms for Eulerian finite difference methods, unpublished.
- Fedkiw, R.P., Aslam, T., Merriman, B., Osher, S., 1999. A non-oscillatory Eulerian approach to interfaces in multimaterial flows (the ghost fluid method). *Journal of Computational Physics* 152, 457–492.
- Godunov, S.K., 1959. A difference method for the numerical calculation of discontinuous solutions of hydrodynamic equations. *Mathematics of the USSR—Sbornik* 47, 271.
- Grove, J.W., Menikoff, R., 1990. Anomalous reflection of a shock wave at a fluid interface. *Journal of Fluid Mechanics* 219, 313–336.
- Haas, J.-F., Sturtevant, B., 1987. Interaction of weak shock waves with cylindrical and spherical gas inhomogeneities. *Journal of Fluid Mechanics* 181, 41–76.
- Henderson, L.-F., 1966. The refraction of a plane shock wave at a gas interface. *Journal of Fluid Mechanics* 26, 607.
- Henderson, L.-F., 1989. On the refraction of shock waves. *Journal of Fluid Mechanics* 198, 365–386.
- Henderson, L.-F., Colella, P., Puckett, E.G., 1991. On the refraction of shock waves at a slow–fast gas interface. *Journal of Fluid Mechanics* 224, 1–27.
- Igra, D., Takayama, K., 2003. Experimental investigation of two cylindrical water columns subjected to planar shock wave loading. *Journal of Fluids Engineering* 125, 325–331.
- Jahn, L.-F., 1956. The refraction of shock waves at a gaseous interface. *Journal of Fluid Mechanics* 1, 457.
- Landau, L.D., Lifschitz, E.M., 1988. *Theoretical Physics, fourth ed. Mechanics, vol. 1*. Nauka, Moscow.
- Liu, T.G., Khoo, B.C., Yeo, K.S., 2001. The simulation of compressible multi-medium flow. II. Applications to 2D underwater shock refraction. *Computers & Fluids* 30, 315–337.
- Nourgaliev, R.R., Dinh, T.N., Suschikh, S.Yu., Yuen, W.W., Theofanous, T.G., 2003. The characteristics-based matching method for compressible flow in complex geometries. AIAA 2003-0247, Presented at the 41st AIAA Aerospace Sciences Meeting and Exhibit, January 6–9, 2003, Reno, NV, USA.
- Nourgaliev, R.R., Dinh, T.N., Theofanous, T.G., Koning, J.M., Greenman, R.M., Nakafuji, G.T., 2004a. Direct numerical simulation of disperse multiphase high-speed flows. AIAA 2004-1284, Presented at the 42nd AIAA Aerospace Sciences Meeting and Exhibit, January 5–8, 2004, Reno, NV, USA.
- Nourgaliev, R.R., Dinh, T.N., Theofanous, T.G., 2004b. The ‘characteristics-based matching’ (CBM) method for compressible flow with moving boundaries and interfaces. *ASME Journal of Fluids Engineering* 126, 586–604.
- Nourgaliev, R.R., Dinh, T.N., Theofanous, T.G., 2004c. Direct numerical simulation of compressible multiphase flows: interaction of shock waves with dispersed multimaterial media. In: *CD-ROM Proceedings of the 5th International Conference on Multiphase Flow, ICMF’04*, Yokohama, Japan, May 30–June 4, 2004, Paper No. 494.
- Nourgaliev, R.R., Dinh, T.N., Theofanous, T.G., 2005a. Adaptive characteristics-based matching for compressible multifluid dynamics. *Journal of Computational Physics*, submitted for publication.

- Nourgaliev, R.R., Wiri, S., Dinh, T.N., Theofanous, T.G., 2005b. On improving mass conservation of level set method by reducing spatial discretization errors. *International Journal of Multiphase Flows*, submitted for publication.
- Peng, D.P., Merriman, B., Osher, S., Zhao, H., Kang, M., 1999. A PDE-based fast local level set method. *Journal of Computational Physics* 155, 410–438.
- Quirk, J.J., Karni, S., 1996. On the dynamics of a shock–bubble interaction. *Journal of Fluid Mechanics* 318, 129–163.
- Schwendeman, D.W., 1988. Numerical shock propagation in non-uniform media. *Journal of Fluid Mechanics* 188, 383–410.
- Takayama, K., 1987. Holographic interferometric study of shock wave propagation in two-phase media in shock tubes and waves. In: *Proceedings of the Sixteenth International Symposium on Shock Tubes and Waves*, Aachen, West Germany, July 26–31, 1987, pp. 51–62.
- Theofanous, T.G., Nourgaliev, R.R., Dinh, T.N., 2004. Compressible multi-hydrodynamics: mixing, dispersal, dissemination of liquids/solids in high speed flows. In: *IUTAM Symposium on “Computational Approaches to Disperse Multiphase Flow”*, Argonne National Laboratory, Argonne, Illinois, October 4–7, 2004, in press.
- Tulin, M.P., 1969. On the creation of ultra-jets. In: Block, I.E. (Ed.), *Problems of Hydrodynamics and Continuum Mechanics: To the 60th Birthday of Academician L.I. Sedov*. SIAM, NY, pp. 465–482.
- van Leer, B., 1979. Towards the ultimate conservative difference scheme, a second order sequel to Godunov’s method. *Journal of Computational Physics* 32, 101–136.
- von Neumann, J., 1943. In: *Collected Works*, vol. 6. Pergamon (1963).
- Whitham, G.B., 1958. On the propagation of shock waves through regions of non-uniform area or flow. *Journal of Fluid Mechanics* 4, 337–360.
- Whitham, G.B., 1959. A new approach to problems of shock dynamics. 2-, 3-Dimensional problems. *Journal of Fluid Mechanics* 5, 369–386.
- Wissink, A.M., Hornung, R., 2004. SAMRAI: a framework for developing parallel AMR applications. In: *5th Symposium on Overset Grids and Solution Technology*, Davis, CA, September 18–20, 2000. Also available as LLNL technical report UCRL-VG-140369.